Nano Research
2022, 15(3): 2667–2673

ISSN 1998-0124 CN 11-5974/O4
https://doi.org/10.1007/s12274-021-3730-3

Research Article

Few-layered organic single-crystalline heterojunctions for high-performance phototransistors

Xinzi Tian[1], Jiarong Yao[1], Lijuan Zhang[1], Bin Han[1], Jianwei Shi[3], Jianwei Su[4], Jie Liu[5], Chunlei Li[5], Xinfeng Liu[3] (✉), Tianyou Zhai[4], Lang Jiang[5], Fangxu Yang[1], Xiaotao Zhang[1], Ye Zou[5], Rongjin Li[1] (✉), and Wenping Hu[1,2,5]

[1] *Tianjin Key Laboratory of Molecular Optoelectronic Sciences, Department of Chemistry, School of Science, Tianjin University, Tianjin 300072, China*
[2] *Joint School of National University of Singapore and Tianjin University, International Campus of Tianjin University, Binhai New City, Fuzhou 350207, China*
[3] *CAS Key Laboratory of Standardization and Measurement for Nanotechnology, CAS Center for Excellence in Nanoscience, National Center for Nanoscience and Technology, Beijing 100190, China*
[4] *State Key Laboratory of Materials Processing and Die & Mould Technology, School of Materials Science and Engineering, Huazhong University of Science and Technology (HUST), Wuhan 430074, China*
[5] *National Laboratory for Molecular Sciences, Key Laboratory of Organic Solids, Institute of Chemistry, Chinese Academy of Sciences, Beijing 100190, China*

Received: 22 April 2021 / **Revised:** 28 June 2021 / **Accepted:** 3 July 2021

ABSTRACT

Photogating and electrical gating are key physical mechanisms in organic phototransistors (OPTs). However, most OPTs are based on thick and polycrystalline films, which leads to substantially low efficiency of both photogating and electrical gating and thus reduced photoresponse. Herein, high-performance OPTs based on few-layered organic single-crystalline heterojunctions are proposed and the obstacle of thick and polycrystalline films for photodetection is overcome. Because of the molecular scale thickness of the type I organic single-crystalline heterojunctions in OPTs, both photogating and electrical gating are highly efficient. By synergy of efficient photogating and electrical gating, key figures of merit of OPTs reach the highest among those based on planar heterojunctions so far as we know. The production of few-layered organic single-crystalline heterojunctions will provide a new type of advanced materials for various applications.

KEYWORDS

two-dimensional (2D) molecular crystals, organic single crystals, organic heterojunctions, organic phototransistors

1 Introduction

Efficient photodetection is essential in modern science and technology. Organic photodetectors (OPDs) have attracted considerable attention because they can be fabricated on mechanically flexible and/or large surfaces by solution processing techniques. Moreover, color selectivity without color filters can be achieved by selecting organic semiconductors with tailorable optoelectronic properties. As a result, OPDs have shown great potential in next-generation imaging, health monitoring, optical communication, biomedical detection and so on [1–6].

There are several requirements to fabricate high-performance OPDs, such as high external quantum efficiency (EQE), high photoconductive gain (G) and low dark current (I_{dark}). High EQE and high G ensure high responsivity (R). Low I_{dark} together with high R results in high photosensitivity (P) and specific detectivity (D^*) [7]. Organic phototransistors (OPTs) with planar heterojunctions as the photoactive layers are a type of promising device structure for highly sensitive photodetection [8–12]. The reasons are threefold. First, the heterojunctions help the dissociation of excitons into free charge carriers. Because of the low dielectric constants of organic materials (static ε = 3–4), the exciton binding energy is large (0.3–0.5 eV) and the efficiency of exciton dissociation in pristine organic semiconductors is low [13–16]. In contrast, photogenerated excitons can be dissociated efficiently at the interfaces of heterojunctions with the help of the built-in potential, resulting in high EQE [17–19]. Second, the free charge carriers can recirculate in the channels of OPTs many times before recombination, producing high G. Third, a gate voltage can be applied to reduce the conductivity of the channel, resulting in low I_{dark}. As a result, heterojunction OPTs have attracted immense attention in recent years [8–10]. For example, in 2013, Wang et al. designed OPTs based on heterojunctions composed of polycrystalline films of copper phthalocyanine (CuPc, 50 nm) and lead phthalocyanine (PbPc, 15 nm). The maximum P and R reached 6.2 × 10^2 and 77.4 mA·W^{-1}, respectively [20]. Recently, in 2018, Peng et al. designed OPTs based on heterojunctions composed of pentacene (30 nm)/tin phthalocyanine (SnPc, 20 nm) films. The maximum P, R, and D^* reached 83.6, 1.0 A·W^{-1}, and 3.1 × 10^{11} Jones, respectively [21].

Photogating and electrical gating are key physical mechanisms in OPTs. However, most of the reported works used thermal

Address correspondence to Xinfeng Liu, liuxf@nanoctr.cn; Rongjin Li, lirj@tju.edu.cn

evaporation or spin coating techniques to prepare polycrystalline films as the photoactive layers. Also, the thicknesses were typically several tens of nanometers to achieve continuous films for charge collection (Table S1 in the Electronic Supplementary Material (ESM)). There were two problems of thick and polycrystalline photoactive layers for OPTs. First, both photogating and electrical gating were inefficient in thick films because of the interlayer shielding effect (see the detail information in the ESM) [7, 22–25]. Second, both the electron (and/or hole) mobility and exciton mobility were reduced in polycrystalline films because of the high density of defects (e.g., grain boundaries) [24, 26]. As a result, thick and polycrystalline photoactive layers led to substantially low efficiency of both photogating and electrical gating and thus reduced photoresponse. In principle, the problems could be overcome by few-layered organic single-crystalline heterojunctions, which were expected to show efficient photogating and electrical gating effect and thus superior performance [7, 24, 27]. However, the obstacle to construct such ultra-thin photoactive channels blocked the way. Up to now, the intrinsic structural problems of thick and polycrystalline photoactive layers were unavoidable and have become a bottleneck in the development of OPTs.

Herein, OPTs based on few-layered organic single-crystalline heterojunctions were proposed and the obstacle of thick and polycrystalline films for photodetection was overcome. Ultra-thin organic single-crystalline heterojunctions were produced by the growth of semi-freestanding two-dimensional molecular crystals (2DMCs) [28–34] on a liquid surface following by layer-by-layer transfer on the target substrate. Because of the molecular scale thickness of the 2DMCs and their formation of type I heterojunctions, both photogating and electrical gating were highly efficient. The synergy of efficient photogating and electrical gating resulted in high EQE, high G and low I_{dark}. As a result, OPTs showed a high R up to 891.4 A·W^{-1}, P up to 5.9 × 10^{7}, EQE up to 3.03 × 10^{5} and D^* up to 2.5 × 10^{16} Jones, all of which were the highest values among OPTs based on planar heterojunctions as far as we know (Table S1 in the ESM).

2 Experimental

2.1 Substrates modification

SiO_2/Si wafers with 300 nm-thick SiO_2 were used as the substrates. The wafers were cleaned sequentially with deionized water, acetone, and isopropanol and then cleaned with oxygen plasma for 10 min. The cleaned wafers were immediately modified with octadecyltrichlorosilane (OTS) by a vapor phase method. The OTS-modified substrates were cleaned by sonification in chloroform, n-hexane and isopropanol, successively.

2.2 Materials and instrumentations

6,13-bis(triisopropylsilylethynyl)pentacene (TIPS-PEN) was purchased from TCI. 2,6-bis(4-hexylphenyl)anthracene (C6-DPA) was purchased from Shanghai Daeyeon Chemicals. Both compounds were used without purification. Optical microscope (OM) and polarized optical microscope (POM) images were taken with a Nikon ECLIPSE Ci-POL polarized optical microscope. Transmission electronic microscopy (TEM) and selected area electron diffraction (SAED) measurements were conducted on a Tecnai G2 F20 S-TWIN transmission electron microscope. Tapping mode atomic force microscopy (AFM) was performed using a Bruker Dimension Icon. High-resolution atomic force microscope (HRAFM) was performed using a Cypher ES. Ultraviolet photoelectron spectrometer (UPS) characterizations were performed on an AXIS ULTRA DLD photoelectron spectroscopy (Kratos, UK) with an unfiltered He discharge lamp (21.2 eV) as the excitation source. Photoluminescence (PL) measurements were carried out using a Confocal Smart Raman system with 405 nm laser excitation. OPTs were measured in the air at room temperature using a probe station connected to a Keithley 4200-SCS. The photoelectrical responses were studied by a 365 nm laser generator with tunable power density from 17.0 to 37.4 μW·cm^{-2}. X-ray diffraction (XRD) measurements were carried out in reflection mode at 45 kV and 200 mA with monochromatic Cu Kα radiation utilizing a Rigaku Smartlab diffractometer. The ultraviolet–visible (UV–vis) spectra were measured by a SHZMADZU UV-3600 Plus spectrophotometer.

2.3 Device fabrication and characterization

The device was fabricated on an OTS-modified SiO_2 (300 nm)/Si substrate. Bottom-gate and top-contact device configuration was achieved by stamping Au stripes on the heterojunction as the source and drain electrodes. In OPTs, R can be evaluated by $R = (I_{light} - I_{dark})/P_{in}$, where I_{light} and I_{dark} are the drain currents under laser irradiation and dark condition, P_{in} is the power density of incident photons. EQE can be defined as EQE = Rhv/e, where e is the unit electron charge and hv represents the energy of one single photon. The P can be calculated by the equation $P = (I_{light} - I_{dark})/I_{dark}$. D^* is defined as $D^* = R(AB)^{1/2}/i_{noise}$, where i_{noise} is the noise current; A is the sensing area of active and B is bandwidth. All reports in Table S1 in the ESM assumed that the shot noise from the dark current was the main contribution of noise current. In this case D^* can be expressed as $D^* = RA^{1/2}/(2qI_{dark})^{1/2}$.

3 Results and discussion

Several strategies including drop casting [34], physical vapor transport [35], solution shearing [36, 37], and bar-coating [38] have been reported for the production of molecularly thin 2DMCs on solid substrates. However, because of the molecular scale thickness of the 2DMCs, it was challenging to peel them off from solid substrates for the construction of heterojunctions. We have recently developed the "layer defining strategy" to grow 2DMCs on glycerol surface [22]. One key advantage of the "layer defining strategy" is that 2DMCs are grown on a liquid surface and the 2DMCs are semi-freestanding. Thus, it is possible to transfer the 2DMCs layer by layer to construct heterojunctions.

In this study, two exemplary organic semiconductors, i.e., C6-DPA and TIPS-PEN (insets of Figs. S1(a) and S1(d) in the ESM) were selected as the architype materials because they showed good solubility, high stability and high mobility in organic field-effect transistors (OFETs) [33, 39, 40]. Taking advantage of the "layer defining strategy" [22], few-layered organic single-crystalline heterojunctions based on 2DMCs were produced successfully. First, 2DMCs of TIPS-PEN were grown on the surface of glycerol and transferred onto an OTS-modified SiO_2/Si substrate. Then, 2DMCs of C6-DPA were grown by the same method. Finally, 2DMCs of C6-DPA floating on the surface of glycerol were transferred onto the OTS-modified SiO_2/Si substrate pre-covered by 2DMCs of TIPS-PEN to form the few-layered single-crystalline heterojunctions (Fig. S1 in ESM).

OM images of both 2DMCs transferred to OTS-modified SiO_2/Si substrates were shown in Figs. 1(a) and 1(d), respectively. These crystals exhibited smooth surfaces without any notable steps. The areas of these crystals were larger than 10^4 μm^2. Under a POM, the color of the entire films changed uniformly from bright to dark when the 2DMCs were rotated 45°, indicating that there were no grain boundaries (Figs. 1(b), 1(c), 1(e), and 1(f)). In Fig. 1(g), a 2DMC of TIPS-PEN was covered by a 2DMC of C6-DPA, forming a heterojunction with an area larger than 10^4 μm^2.

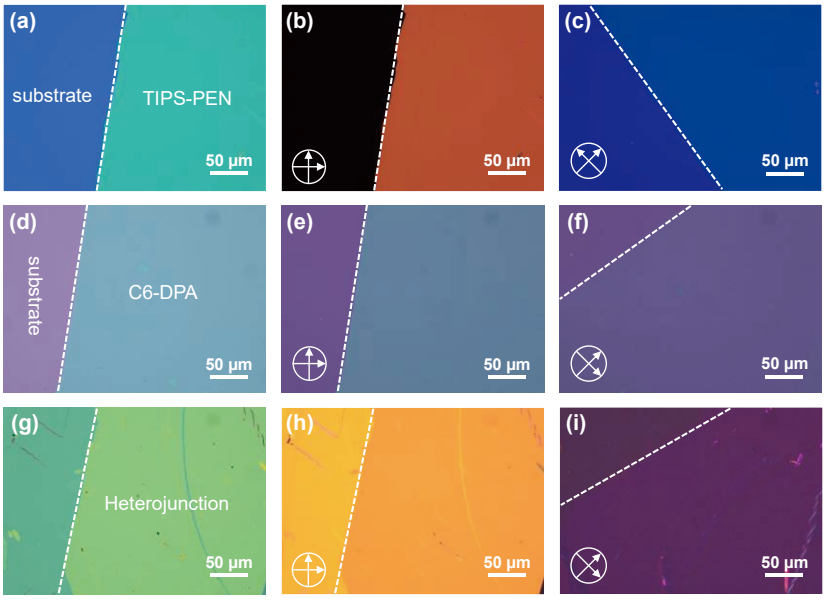

Figure 1 OM images of both 2DMCs and their heterojunctions. OM images of 2DMCs of (a) TIPS-PEN, (d) C6-DPA and (g) their heterojunctions, respectively. (b) and (c) POM images of 2DMCs of TIPS-PEN. (e) and (f) POM images of 2DMCs of C6-DPA. (h) and (i) POM images of heterojunctions.

The color of the heterojunction region changed uniformly from bright to dark under a POM when the substrate was rotated by 45° (Figs. 1(h) and 1(i)), indicating the successful production of a single-crystalline heterojunction.

XRD patterns (Fig. S2 in the ESM) and UV–vis absorption spectra (Fig. S3 in the ESM) of the heterojunctions showed all the characteristic peaks of the single components, indicating the successful preparation of the single-crystalline heterojunctions. Figures 2(a) and 2(b) show typical AFM images of 2DMCs of TIPS-PEN and C6-DPA. The thicknesses were 10.1 and 7.1 nm, respectively, corresponding to 6 and 2 molecule layers (Figs. 2(d) and 2(e)). The root mean square (RMS) roughness of 2DMCs of TIPS-PEN and C6-DPA was 0.25 and 0.17 nm, respectively. The atomically flat surfaces not only indicated the single-crystalline nature of the 2DMCs, but also ensured the intimate layer by layer vertical stacking for few-layered single-crystalline heterojunctions. An AFM image of a heterojunction is shown in Fig. 2(c). Clear boundaries and overlapping of the two 2DMCs were observed. As shown in Fig. 2(f), the thickness of the heterojunction was 16.3 nm, which coincided with a sum of the thicknesses of 2DMCs of C6-DPA (6.9 nm) and TIPS-PEN (9.5 nm). Owing to the atomically flat surfaces of the component 2DMCs, the surface of the few-layered single-crystalline heterojunctions was uniform and flat (RMS = 0.46 nm). The atomically flat surfaces of the component 2DMCs also ensured sharp interfaces of the heterojunctions, which were essential for high-performance optoelectronic devices [41, 42]. TEM images and SAED patterns of TIPS-PEN and C6-DPA crystals are shown in Figs. 2(g) and 2(i). The TEM images of both 2DMCs showed uniform morphology (the insets of Figs. 2(g) and 2(i)), and the corresponding SAED patterns exhibited ordered diffraction spots, confirming the single-crystalline nature of both films. HRAFM images were further performed to assess the crystallinity of both 2DMCs. Figures 2(h) and 2(j) show the molecular packing of TIPS-PEN and C6-DPA in the heterojunctions. Lattice constants of a = 7.61 Å, b = 7.75 Å, and θ = 83.6° for TIPS-PEN and a = 6.36 Å, b = 8.13 Å, and θ = 86.5° for C6-DPA were obtained, which coincided with previous reports [22, 43]. The high-quality single-crystalline 2DMCs laid the foundation to construct few-layered organic single-crystalline heterojunctions for high-performance OPTs.

The photoelectrical properties of the few-layered organic single-crystalline heterojunctions were investigated by the construction of OPTs with a bottom-gate top-contact configuration (Fig. 3(a)). The OFETs based on pristine 2DMCs of TIPS-PEN and the few-layered single-crystalline heterojunctions were discussed in Fig. S4 in the ESM. Au (80 nm) was used as source and drain electrodes and OTS-modified SiO_2 (300 nm)/Si as gate dielectric layer. All measurements were carried out in ambient air at room temperature. Figure 3(b) shows the typical transfer characteristics of the OPTs measured in dark and under 365 nm laser irradiation with different intensities. By increasing the laser power intensity from 17.0 to 37.4 μW·cm^{-2}, the transfer curves shifted upward prominently to higher source-drain current and the threshold voltage (V_{th}) shifted towards more positive values (Fig. 3(c)), indicating a prominent photoresponse. Compared with OPTs based on pristine 2DMC of TIPS-PEN and 2DMC of C6-DPA, a dramatic improvement of the performance was observed for devices based on few-layered single-crystalline heterojunctions with a maximum P of 5.9 × 10^{7} and D^* of 2.5 × 10^{16} Jones (Figs. 3(d) and 3(e)). It was noted that P and D^* values were about 6 times and 3 times higher than those of pristine 2DMC of TIPS-PEN (Fig. S5 in the ESM). And the P and D^* values were increased by about 1 order of magnitude compared to those of 2DMC of C6-DPA (Fig. S6 in the ESM). Moreover, a maximum R of 891.4 A·W^{-1} was obtained (Fig. 3(f)), which were about 9 times higher than that of pristine 2DMC of TIPS-PEN (94.1 A·W^{-1}) and six times higher than that of pristine 2DMC of C6-DPA (135.8 A·W^{-1}). The R, P and D^* values of OPTs based on few-layered single-crystalline heterojunction were all higher than that of the 2DMCs of TIPS-PEN and C6-DPA. All these parameters were competitive among OPTs based on organic single crystals reported so far (Table S2 in ESM). Notably, the R, P and D^* values were the highest among OPTs based on planar heterojunctions so far as we know. Specifically, the D^* value was three orders of magnitude higher than those from previous reports (Table S1 in the ESM).

To elucidate the origin of the high photoresponse of the few-layered single-crystalline heterojunctions, PL emission spectroscopy and PL mapping were carried out (Figs. 4(a) and 4(b)). Typical PL spectra collected in the 2DMC of C6-DPA and the few-layered single-crystalline heterojunction are shown in Fig. 4(a), where three strong exciton peaks at 442, 470 and 504 nm (at excitation wavelength of 405 nm) belonging to C6-DPA were

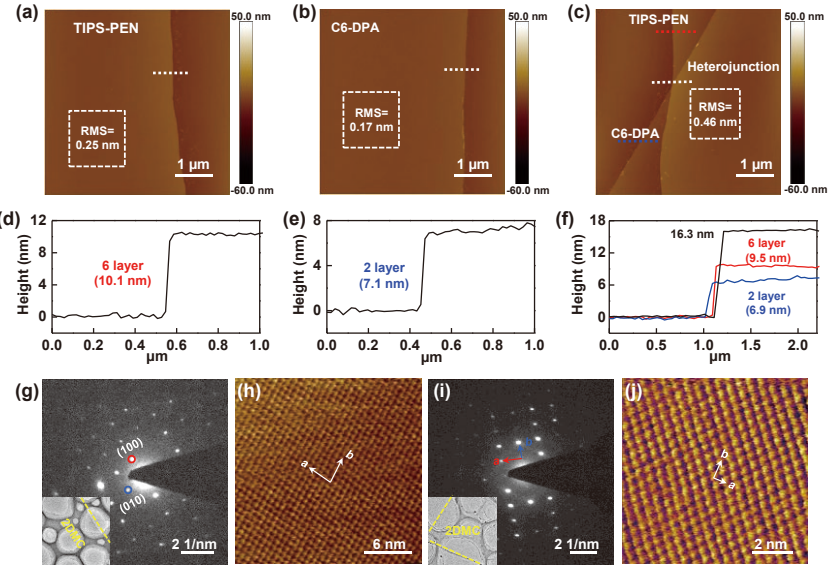

Figure 2 Surface morphologies and single-crystalline structures characterization of 2DMCs. AFM images of 2DMCs of (a) TIPS-PEN, (b) C6-DPA, and (c) their heterojunctions, respectively. (d) Height profiles of 2DMCs of TIPS-PEN, (e) C6-DPA, and (f) their heterojunctions, respectively. (g) TEM image and the corresponding SAED pattern of a 2DMC of TIPS-PEN. (h) HRAFM image of a 2DMC of TIPS-PEN. (i) TEM image and the corresponding SAED pattern of a 2DMC of C6-DPA. (j) HRAFM image of a 2DMC of C6-DPA.

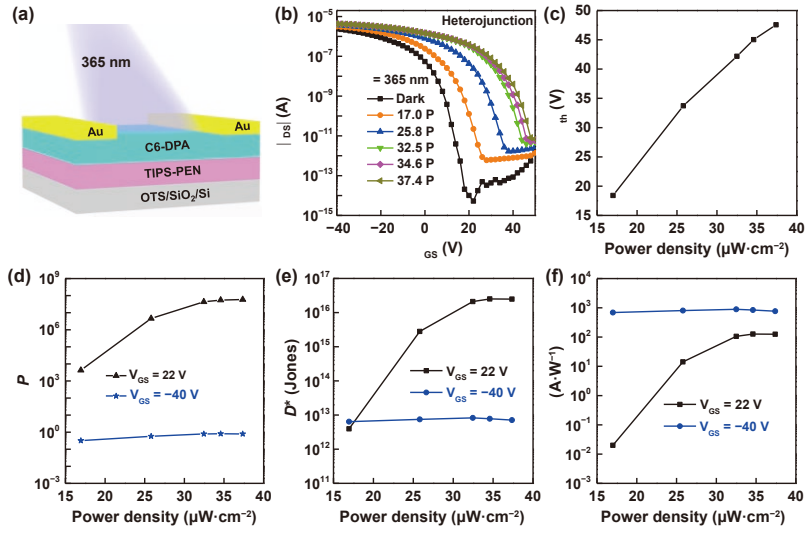

Figure 3 Photoelectrical properties of organic single-crystalline heterojunctions. (a) Device structure of the OPTs based on few-layered single-crystalline heterojunctions under 365 nm laser irradiation. (b) Transfer curves of an OPT with V_{DS} = −40 V under dark condition and different laser intensities (1 P = 1 μW·cm^{-2}). (c) Laser intensities dependence of the threshold voltage (V_{th}). (d) P and (e) D^* of the OPT as a function of laser intensities. The maximum P and D^* values were obtained under 365 nm laser with power density of 37.4 μW·cm^{-2} and V_{GS} = 22 V. (f) R of the OPT as a function of laser intensities. The maximum R was obtained under 365 nm laser with power density of 32.5 μW·cm^{-2} and V_{GS} = −40 V.

identified [44, 45]. The PL spectrum of 2DMC of TIPS-PEN is shown in Fig. S7 in the ESM. Figure 4(b) shows the PL intensity mapping of the C6-DPA and the few-layered single-crystalline heterojunction (at wavelength of 500–550 nm). The C6-DPA region exhibited strong PL emission, whereas the few-layered single-crystalline heterojunction region showed apparent PL quenching. Judging from Figs. 4(a) and 4(b), the PL intensity of C6-DPA was significantly decreased in the heterojunction, which could be ascribed to photoexcited charge transfer from C6-DPA to TIPS-PEN [46–48]. To confirm the photoexcited charge transfer in the heterojunctions, the energy levels of both 2DMCs were determined by UPS (Figs. S8 and S9 in the ESM). The highest occupied molecular orbital (HOMO) levels of TIPS-PEN and C6-DPA were −5.18 and −5.60 eV, respectively. The lowest unoccupied molecular orbital (LUMO) levels calculated from their HOMO levels and optical energy band gaps were −3.52 and −2.84 eV, respectively [49]. A type I heterojunction was formed when two materials were brought into contact (Fig. 4(c)). Excitons were generated in C6-DPA under laser irradiation (λ = 365 nm) and the heterojunction helped the dissociation of the excitons into free electrons and holes, leading to high EQE [50]. The HOMO of C6-DPA was about 0.42 eV lower than that of TIPS-PEN (ΔHOMO = 0.42 eV). Thus, photogenerated free holes were transferred from C6-DPA to TIPS-PEN. These free holes circulated in TIPS-PEN layer under a bias voltage (V_{DS}), producing photocurrent. The LUMO of TIPS-PEN was 0.68 eV lower than that of C6-DPA (ΔLUMO = 0.68 eV), which allowed the photogenerated free electrons to transfer from C6-DPA to TIPS-PEN. The ΔLUMO also blocked the reverse flow of free electrons from TIPS-PEN to C6-DPA. Considering that TIPS-PEN was a p-type semiconductor with electron-trap states, the transferred electrons were trapped at the interface in the TIPS-PEN layer (Fig. 4(c)). The trapped electrons produced an electric-field like gate voltage to modulate the channel conductance. Judging from the above

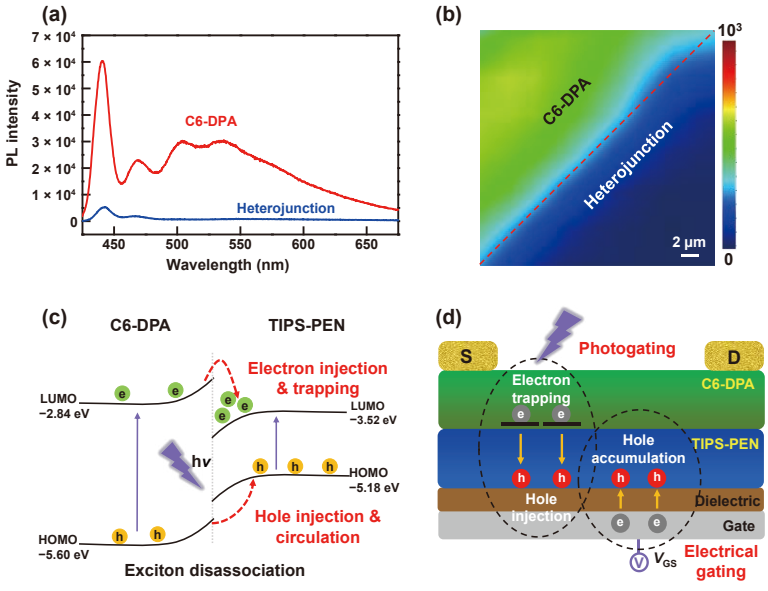

Figure 4 PL spectra and schematic diagram of mechanism. (a) PL spectra of 2DMC of C6-DPA and the few-layered single-crystalline heterojunction. (b) PL intensity mapping (500–550 nm) of 2DMC of C6-DPA and the few-layered single-crystalline heterojunction. (c) Energy band alignment and charge transfer process of the few-layered single-crystalline heterojunction under irradiation. (d) Schematic of photogating and electrical gating in the few-layered single-crystalline heterojunction under irradiation.

analysis, C6-DPA served as the photogate and TIPS-PEN worked as the channel in the OPTs (Fig. 4(d)). The photogating effect was efficient in molecularly-thin 2D materials because of the large capacitance due to a short distance between the photogate and the channel [24, 27]. The efficient photogating was proven by Figs. 3(b) and 3(c), where the transfer curves shifted notably to the positive direction by laser irradiation, suggesting an immense negative gating induced by trapped electrons [24, 51]. Such an efficient photogating was favorable for high G [27, 52]. Meanwhile, electrical gating was also efficient because of the elimination of the interlayer shielding effect in molecularly-thin 2DMCs [7, 22–25]. In the dark, the channel could be fully depleted by a positive gate voltage [7], resulting in extremely low I_{dark} of 5.2×10^{-15} A (Fig. 3(b), 3–4 orders or lower than previous reports, see Table S1 in the ESM). Under irradiation, mobile holes were induced and accumulated in TIPS-PEN by the application of a negative gate voltage, leading to a large photocurrent (Fig. 4(d)). In a word, by synergy of efficient photogating and electrical gating in the few-layered organic single-crystalline heterojunctions, a high EQE, a high G and a low I_{dark} were achieved, all of which ensured high-performance OPTs.

4 Conclusions

We proposed few-layered organic single-crystalline heterojunctions to obtain high-performance OPTs. Because of the molecular scale thickness of the 2DMCs and their formation of type I heterojunctions in OPTs, both photogating and electrical gating were highly efficient. By synergy of efficient photogating and electrical gating, the OPTs showed a high R up to 891.4 A·W^{-1}, P up to 5.9×10^{7}, EQE up to 3.03×10^{5} and D^{*} up to 2.5×10^{16} Jones, all of which were the highest values among OPTs based on planar heterojunctions as far as we know. We believe the general strategy for the construction of few-layered organic single-crystalline heterojunctions will provide a new type of advanced materials towards various high-performance optoelectronic devices.

Acknowledgements

The authors acknowledge the financial support from the National Natural Science Foundation of China (Nos. 51873148, 52073206, 51633006, and 61704038), the Natural Science Foundation of Tianjin City (No. 18JC-YBJC18400), and Strategic Priority Research Program of Chinese Academy of Sciences (XDB36000000).

Electronic Supplementary Material: Supplementary material (XRD measurements, UV–vis absorption spectroscopy, OFETs based on pristine 2DMCs of TIPS-PEN and the few-layered single-crystalline heterojunctions, OPTs based on 2DMCs of TIPS-PEN and C6-DPA, PL spectra of 2DMC of TIPS-PEN, UPS spectra of the TIPS-PEN and C6-DPA) is available in the online version of this article at https://doi.org/10.1007/s12274-021-3730-3.

References

[1] Tang, Q.; Zhang, G. P.; Jiang, B. H.; Ji, D. Y.; Kong, H. H.; Riehemann, K.; Ji, Q. M.; Fuchs, H. Self-assembled fullerene (C_{60})-pentacene superstructures for photodetectors. *SmartMat* **2021**, *2*, 109–118.

[2] Chow, P. C. Y.; Someya, T. Organic photodetectors for next-generation wearable electronics. *Adv. Mater.* **2020**, *32*, 1902045.

[3] Yao, Y. F.; Chen, Y. S.; Wang, H. L.; Samorì, P. Organic photodetectors based on supramolecular nanostructures. *SmartMat* **2020**, *1*, e1009.

[4] Yang, F. X.; Cheng, S. S.; Zhang, X. T.; Ren, X. C.; Li, R. J.; Dong, H. L.; Hu, W. P. 2D organic materials for optoelectronic applications. *Adv. Mater.* **2018**, *30*, 1702415.

[5] He, X. W.; Léonard, F.; Kono, J. Uncooled carbon nanotube photodetectors. *Adv. Opt. Mater.* **2015**, *3*, 989–1011.

[6] Kuribara, K.; Wang, H.; Uchiyama, N.; Fukuda, K.; Yokota, T.; Zschieschang, U.; Jaye, C.; Fischer, D.; Klauk, H.; Yamamoto, T. et al. Organic transistors with high thermal stability for medical applications. *Nat. Commun.* **2012**, *3*, 723.

[7] Kufer, D.; Konstantatos, G. Photo-FETs: Phototransistors enabled by 2D and 0D nanomaterials. *ACS Photonics* **2016**, *3*, 2197–2210.

[8] Wang, C.; Zhang, X. T.; Hu, W. P. Organic photodiodes and phototransistors toward infrared detection: Materials, devices, and applications. *Chem. Soc. Rev.* **2020**, *49*, 653–670.

[9] Guo, J. H.; Jiang, S.; Pei, M. J.; Xiao, Y. L.; Zhang, B. W.; Wang, Q. J.; Zhu, Y.; Wang, H. Y.; Jie, J. S.; Wang, X. R. et al. Few-layer organic crystalline van der waals heterojunctions for ultrafast UV phototransistors. *Adv. Electron. Mater.* **2020**, *6*, 2000062.

[10] Qian, C.; Sun, J.; Kong, L. A.; Gou, G. Y.; Zhu, M. L.; Yuan, Y. B.; Huang, H.; Gao, Y. L.; Yang, J. L. High-performance organic heterojunction phototransistors based on highly ordered copper phthalocyanine/*para*-sexiphenyl thin films. *Adv. Funct. Mater.* **2017**, *27*, 1604933.
[11] Baeg, K. J.; Binda, M.; Natali, D.; Caironi, M.; Noh, Y. Y. Organic light detectors: Photodiodes and phototransistors. *Adv. Mater.* **2013**, *25*, 4267–4295.
[12] Li, F.; Chen, Y.; Ma, C.; Buttner, U.; Leo, K.; Wu, T. High-performance near-infrared phototransistor based on n-type small-molecular organic semiconductor. *Adv. Electron. Mater.* **2017**, *3*, 1600430.
[13] Mikhnenko, O. V.; Blom, P. W. M.; Nguyen, T. Q. Exciton diffusion in organic semiconductors. *Energy Environ. Sci.* **2015**, *8*, 1867–1888.
[14] Deibel, C.; Strobel, T.; Dyakonov, V. Role of the charge transfer state in organic donor–acceptor solar cells. *Adv. Mater.* **2010**, *22*, 4097–4111.
[15] Brédas, J. L.; Beljonne, D.; Coropceanu, V.; Cornil, J. Charge-transfer and energy-transfer processes in π-conjugated oligomers and polymers: A molecular picture. *Chem. Rev.* **2004**, *104*, 4971–5004.
[16] Scheidler, M.; Lemmer, U.; Kersting, R.; Karg, S.; Riess, W.; Cleve, B.; Mahrt, R. F.; Kurz, H.; Bässler, H.; Göbel, E. O. et al. Monte carlo study of picosecond exciton relaxation and dissociation in poly(phenylenevinylene). *Phys. Rev. B* **1996**, *54*, 5536–5544.
[17] Wang, J.; Han, J. Y.; Chen, X. Q.; Wang, X. R. Design strategies for two-dimensional material photodetectors to enhance device performance. *InfoMat* **2019**, *1*, 33–53.
[18] Cheng, R.; Li, D. H.; Zhou, H. L.; Wang, C.; Yin, A. X.; Jiang, S.; Liu, Y.; Chen, Y.; Huang, Y.; Duan, X. F. Electroluminescence and photocurrent generation from atomically sharp WSe_2/MoS_2 heterojunction p-n diodes. *Nano Lett.* **2014**, *14*, 5590–5597.
[19] Dong, H. L.; Zhu, H. F.; Meng, Q.; Gong, X.; Hu, W. P. Organic photoresponse materials and devices. *Chem. Soc. Rev.* **2012**, *41*, 1754–1808.
[20] Peng, Y. Q.; Lv, W. L.; Yao, B.; Fan, G. Y.; Chen, D. Q.; Gao, P. J.; Zhou, M. Q.; Wang, Y. High performance near infrared photosensitive organic field-effect transistors realized by an organic hybrid planar-bulk heterojunction. *Org. Electron.* **2013**, *14*, 1045–1051.
[21] Liang, Y. L.; Lv, W. L.; Luo, X.; He, L.; Xu, K.; Zhao, F. Y.; Huang, F. B.; Lu, F. P.; Peng, Y. Q. A comprehensive investigation of organic active layer structures toward high performance near-infrared phototransistors. *Synth. Met.* **2018**, *240*, 44–51.
[22] Yao, J. R.; Zhang, Y.; Tian, X. Z.; Zhang, X. L.; Zhao, H. J.; Zhang, X. T.; Jie, J. S.; Wang, X. R.; Li, R. J.; Hu, W. P. Layer-defining strategy to grow two-dimensional molecular crystals on a liquid surface down to the monolayer limit. *Angew. Chem., Int. Ed.* **2019**, *58*, 16082–16086.
[23] Wang, C.; Ren, X. C.; Xu, C. H.; Fu, B. B.; Wang, R. H.; Zhang, X. T.; Li, R. J.; Li, H. X.; Dong, H. L.; Zhen, Y. G. et al. N-type 2D organic single crystals for high-performance organic field-effect transistors and near-infrared phototransistors. *Adv. Mater.* **2018**, *30*, 1706260.
[24] Fang, H. H.; Hu, W. D. Photogating in low dimensional photodetectors. *Adv. Sci.* **2017**, *4*, 1700323.
[25] Wang, Q. J.; Qian, J.; Li, Y.; Zhang, Y. H.; He, D. W.; Jiang, S.; Wang, Y.; Wang, X. R.; Pan, L. J.; Wang, J. Z. et al. 2D single-crystalline molecular semiconductors with precise layer definition achieved by floating-coffee-ring-driven assembly. *Adv. Funct. Mater.* **2016**, *26*, 3191–3198.
[26] Menke, S. M.; Holmes, R. J. Exciton diffusion in organic photovoltaic cells. *Energy Environ. Sci.* **2014**, *7*, 499–512.
[27] Buscema, M.; Island, J. O.; Groenendijk, D. J.; Blanter, S. I.; Steele, G. A.; van der Zant, H. S. J.; Castellanos-Gomez, A. Photocurrent generation with two-dimensional van der waals semiconductors. *Chem. Soc. Rev.* **2015**, *44*, 3691–3718.
[28] Wang, C.; Fu, B. B.; Zhang, X. T.; Li, R. J.; Dong, H. L.; Hu, W. P. Solution-processed, large-area, two-dimensional crystals of organic semiconductors for field-effect transistors and phototransistors. *ACS Cent. Sci.* **2020**, *6*, 636–652.
[29] Wang, J. W.; Deng, W.; Wang, W.; Jia, R. F.; Xu, X. Z.; Xiao, Y. L.; Zhang, X. J.; Jie, J. S.; Zhang, X. H. External-force-driven solution epitaxy of large-area 2D organic single crystals for high-performance field-effect transistors. *Nano Res.* **2019**, *12*, 2796–2801.
[30] Qian, J.; Jiang, S.; Li, S. L.; Wang, X. R.; Shi, Y.; Li, Y. Solution-processed 2D molecular crystals: Fabrication techniques, transistor applications, and physics. *Adv. Mater. Technol.* **2019**, *4*, 1800182.
[31] Wang, Q. Q.; Yang, F. X.; Zhang, Y.; Chen, M. X.; Zhang, X. T.; Lei, S. B.; Li, R. J.; Hu, W. P. Space-confined strategy toward large-area two-dimensional single crystals of molecular materials. *J. Am. Chem. Soc.* **2018**, *140*, 5339–5342.
[32] Zhang, Y. H.; Luo, Z. Z.; Hu, F. R.; Nan, H. Y.; Wang, X. Y.; Ni, Z. H.; Xu, J. B.; Shi, Y.; Wang, X. R. Realization of vertical and lateral van der waals heterojunctions using two-dimensional layered organic semiconductors. *Nano Res.* **2017**, *10*, 1336–1344.
[33] Xu, C. H.; He, P.; Liu, J.; Cui, A. J.; Dong, H. L.; Zhen, Y. G.; Chen, W.; Hu, W. P. A general method for growing two-dimensional crystals of organic semiconductors by "solution epitaxy". *Angew. Chem., Int. Ed.* **2016**, *55*, 9519–9523.
[34] Jiang, L.; Dong, H. L.; Meng, Q.; Li, H. X.; He, M.; Wei, Z. M.; He, Y. D.; Hu, W. P. Millimeter-sized molecular monolayer two-dimensional crystals. *Adv. Mater.* **2011**, *23*, 2059–2063.
[35] Wu, B.; Zhao, Y. H.; Nan, H. Y.; Yang, Z. Y.; Zhang, Y. H.; Zhao, H. J.; He, D. W.; Jiang, Z. L.; Liu, X. L.; Li, Y. et al. Precise, self-limited epitaxy of ultrathin organic semiconductors and heterojunctions tailored by van der Waals interactions. *Nano Lett.* **2016**, *16*, 3754–3759.
[36] Peng, B. Y.; Huang, S. Y.; Zhou, Z. W.; Chan, P. K. L. Solution-processed monolayer organic crystals for high-performance field-effect transistors and ultrasensitive gas sensors. *Adv. Funct. Mater.* **2017**, *27*, 1700999.
[37] Becerril, H. A.; Roberts, M. E.; Liu, Z. H.; Locklin, J.; Bao, Z. N. High-performance organic thin-film transistors through solution-sheared deposition of small-molecule organic semiconductors. *Adv. Mater.* **2008**, *20*, 2588–2594.
[38] Zhang, Z. C.; Peng, B. Y.; Ji, X. D.; Pei, K.; Chan, P. K. L. Marangoni-effect-assisted bar-coating method for high-quality organic crystals with compressive and tensile strains. *Adv. Funct. Mater.* **2017**, *27*, 1703443.
[39] Diao, Y.; Tee, B. C. K.; Giri, G.; Xu, J.; Kim, D. H.; Becerril, H. A.; Stoltenberg, R. M.; Lee, T. H.; Xue, G.; Mannsfeld, S. C. B. et al. Solution coating of large-area organic semiconductor thin films with aligned single-crystalline domains. *Nat. Mater.* **2013**, *12*, 665–671.
[40] Xue, G. B.; Fan, C. C.; Wu, J. K.; Liu, S.; Liu, Y. J.; Chen, H. Z.; Xin, H. L.; Li, H. Y. Ambipolar charge transport of TIPS-pentacene single-crystals grown from non-polar solvents. *Mater. Horiz.* **2015**, *2*, 344–349.
[41] Wu, J. K.; Li, Q. F.; Xue, G. B.; Chen, H. Z.; Li, H. Y. Preparation of single-crystalline heterojunctions for organic electronics. *Adv. Mater.* **2017**, *29*, 1606101.
[42] Zhao, X. M.; Liu, T. J.; Liu, H. L.; Wang, S. R.; Li, X. G.; Zhang, Y. T.; Hou, X. Y.; Liu, Z. L.; Shi, W. D.; Dennis, T. J. S. Organic single-crystalline p–n heterojunctions for high-performance ambipolar field-effect transistors and broadband photodetectors. *ACS Appl. Mater. Interfaces* **2018**, *10*, 42715–42722.
[43] Anthony, J. E.; Brooks, J. S.; Eaton, D. L.; Parkin, S. R. Functionalized pentacene: Improved electronic properties from control of solid-state order. *J. Am. Chem. Soc.* **2001**, *123*, 9482–9483.
[44] Yu, X. X.; Zheng, L.; Li, J. F.; Wang, L.; Han, J. L.; Chen, H. Y.; Zhang, X. T.; Hu, W. P. A new asymmetric anthracene derivative with high mobility. *Sci. China Chem.* **2019**, *62*, 251–255.
[45] Liu, J.; Zhang, H. T.; Dong, H. L.; Meng, L. Q.; Jiang, L. F.; Jiang, L.; Wang, Y.; Yu, J. S.; Sun, Y. M.; Hu, W. P. et al. High mobility emissive organic semiconductor. *Nat. Commun.* **2015**, *6*, 10032.
[46] Yang, T. F.; Wang, X.; Zheng, B. Y.; Qi, Z. Y.; Ma, C.; Fu, Y. H.; Fu, Y. P.; Hautzinger, M. P.; Jiang, Y.; Li, Z. W. et al. Ultrahigh-performance optoelectronics demonstrated in ultrathin perovskite-based vertical semiconductor heterostructures. *ACS Nano* **2019**, *13*, 7996–8003.

[47] Zheng, W. H.; Zheng, B. Y.; Yan, C. L.; Liu, Y.; Sun, X. X.; Qi, Z. Y.; Yang, T. F.; Jiang, Y.; Huang, W.; Fan, P. et al. Direct vapor growth of 2D vertical heterostructures with tunable band alignments and interfacial charge transfer behaviors. *Adv. Sci.* **2019**, *6*, 1802204.

[48] Zhang, L. L.; Sharma, A.; Zhu, Y.; Zhang, Y. H.; Wang, B. W.; Dong, M. H.; Nguyen, H. T.; Wang, Z.; Wen, B.; Cao, Y. J. et al. Efficient and layer-dependent exciton pumping across atomically thin organic–inorganic type-I heterostructures. *Adv. Mater.* **2018**, *30*, 1803986.

[49] Li, J.; Zhou, K.; Liu, J.; Zhen, Y. G.; Liu, L.; Zhang, J. D.; Dong, H. L.; Zhang, X. T.; Jiang, L.; Hu, W. P. Aromatic extension at 2, 6-positions of anthracene toward an elegant strategy for organic semiconductors with efficient charge transport and strong solid state emission. *J. Am. Chem. Soc.* **2017**, *139*, 17261–17264.

[50] Singh, J.; Narayan, M.; Ompong, D.; Zhu, F. R. Dissociation of charge transfer excitons at the donor–acceptor interface in bulk heterojunction organic solar cells. *J. Mater. Sci: Mater. Electron.* **2017**, *28*, 7095–7099.

[51] Gao, Y. H.; Yi, Y.; Wang, X. W.; Meng, H.; Lei, D. Y.; Yu, X. F.; Chu, P. K.; Li, J. A novel hybrid-layered organic phototransistor enables efficient intermolecular charge transfer and carrier transport for ultrasensitive photodetection. *Adv. Mater.* **2019**, *31*, 1900763.

[52] Qi, Z. Y.; Yang, T. F.; Li, D.; Li, H. L.; Wang, X.; Zhang, X. H.; Li, F.; Zheng, W. H.; Fan, P.; Zhuang, X. J. et al. High-responsivity two-dimensional p-PbI_2/n-WS_2 vertical heterostructure photodetectors enhanced by photogating effect. *Mater. Horiz.* **2019**, *6*, 1474–1480.